ChemComm

COMMUNICATION

View Article Online
View Journal | View Issue

Cite this: *Chem. Commun.*, 2020, **56**, 7905

Received 14th February 2020,
Accepted 4th June 2020

DOI: 10.1039/d0cc01186j

rsc.li/chemcomm

Stable metal–organic frameworks with low water affinity built from methyl-siloxane linkers†

Luke C. Delmas, [a] Andrew J. P. White,[a] David Pugh, [b] Arwyn Evans,[c] Mark Antonin Isbell,[c] Jerry Y. Y. Heng, [c] Paul D. Lickiss [a] and Robert P. Davies *[a]

A tetracarboxylic acid with a methyl-substituted siloxane core (L-H_4) has been prepared and applied in the construction of water stable MOFs with low water affinity. L-H_4 itself crystallizes as an interpenetrated 3D hydrogen-bonded network. Reaction of L-H_4 with Zr^{IV}/Hf^{IV} gave IMP-32-Zr/Hf – both 3D MOFs of scu topology.

Metal–organic frameworks (MOFs) have been identified as having high potential for environmental clean-up applications including CO_2 capture, hydrocarbon separations, oil spill clean-up, and water purification.[1,2] This is due to their high porosity and tuneable pore shape/size and functionality.[3] However, such clean-up operations require the deployment of MOFs in wet or humid conditions and consequently the hydrothermal stability and water affinity of these materials is often a limiting factor for their commercial use.[4]

Research on the development of hydrophobic MOF materials has mainly focussed on particle coating and linker design strategies.[5] The former involves coating the pristine MOF particles with hydrophobic polymers (such as polydimethylsiloxane) but this requires post-synthetic processing and usually comes at the expense of reduced pore volumes.[6–9] Efforts towards the design of MOF linkers with hydrophobic functionality have focussed on appending hydrophobic groups (*e.g.* CH_3, CF_3, or F) to the linker backbone. Perfluorination has proven to be particularly effective in imparting MOFs with water-repelling properties.[10] However, the synthetic difficulty of fluorination, reduced thermal stability of perfluorinated frameworks,[11–13] and growing concerns over the negative health impact of polyfluoroalkyl substances[14] all stimulate research into alternative methods of linker hydrophobization.

Given our experience in the development of siloxane-based linkers for MOF construction,[15–17] we set out to develop a novel silicone-derived linker for the direct construction of low water affinity MOFs. Silicones are well known for their hydrophobic properties,[18] and studies of post-synthetic incorporation of silicone units in MOF materials [either by particle coating[6–8] or functionalization of secondary building units (SBUs)[19]] suggests that such an approach may successfully lead to low water affinity materials. Siloxane-based linkers compatible with the zirconium oxide family of SBUs were specifically targeted due to the well-established thermal, chemical, and water stabilities of these units.[20] We now report upon the preparation of the novel tetracarboxylic acid linker 1,3-dimethyltetrakis(*p*-carboxyphenyl)disiloxane (**L**-H_4), its application in the preparation of isostructural Zr- and Hf-based frameworks, and studies on the hydrophobicity of these new materials.

The synthesis of **L**-H_4 is outlined in Scheme 1, and is an adaptation of our previously reported protocol for disiloxane-based linker synthesis (see ESI,† for full experimental details).[17] Methylbis(*p*-bromophenyl)silane was prepared from commercially available dichloromethylsilane.

We firstly studied the H-bonded superstructure of the linker itself with crystals of **L**-H_4 suitable for X-ray analysis grown *via* slow evaporation from a mixture of AcOH and MeOH. Extended supramolecular structures built from polycarboxylic acids have recently gained considerable attention since several such materials exhibit permanent porosity and have shown potential for gas separations.[21–23] X-ray analysis reveals that **L**-H_4 crystallizes in the triclinic space group $P\bar{1}$ (no. 2). Free rotation about the Si–O bonds and the flexible Si–O–Si bond angle allows **L**-H_4 to adjust the orientation of its carboxylic acid groups in order to optimise dimeric hydrogen bonding with neighbouring molecules to form an extended structure. The asymmetric unit contains one complete molecule of **L**-H_4 with a bent siloxane linkage [$\angle$Si–O–Si = 148.2(2)°] and half a molecule of **L**-H_4 with

[a] *Molecular Sciences Research Hub, Department of Chemistry, Imperial College London, White City, London, W12 0BZ, UK. E-mail: r.davies@imperial.ac.uk*
[b] *Department of Chemistry, King's College London, Britannia House, 7 Trinity Street, London, SE1 1DB, UK*
[c] *Department of Chemical Engineering, Imperial College London, South Kensington, London, SW7 2AZ, UK*

† Electronic supplementary information (ESI) available: Full synthetic protocol and characterisation data. PXRD, TGA plots, additional topological analysis, and N_2 sorption isotherms for IMP-32 MOFs. CCDC 1950125–1950127. For ESI and crystallographic data in CIF or other electronic format see DOI: 10.1039/d0cc01186j

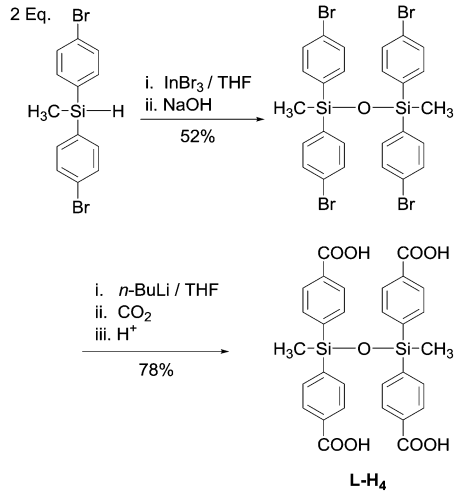

Scheme 1 Synthesis of **L**-H_4.

the central siloxane oxygen sitting on an inversion centre thus giving rise to a linear Si–O–Si linkage [$\angle$Si–O–Si = 180.00(7)°].

Both crystallographically independent molecules are 4-connected supramolecular tectons although with differing geometries. The methyl groups of the linear siloxane molecule are in the antiperiplanar conformation and consequently the coordinating branches in the molecule are disposed with roughly square planar geometry. The methyl groups in the bent siloxane are in the *gauche* conformation with a torsion angle (C–Si···Si–C) of 35.3(2)° resulting in the four *p*-carboxyphenyl arms extending in a highly distorted tetrahedral arrangement. These linear and bent **L**-H_4 molecules are linked *via* dimeric hydrogen-bonding interactions to afford a 3D hydrogen-bonded organic framework (HOF) of **mog** topology (see Fig. 1).

The hydrogen bonding O···O distances all lie in the range 2.58–2.64 Å, typical of the strong hydrogen bonds observed in such carboxylic acid-based HOF systems.[17] Efficient packing in the structure is achieved by mutual interpenetration of three additional **mog** nets and consequently the overall four-fold interpenetrated framework is non-porous with a solvent accessible void of only 2.1% as calculated by the SOLV routine in PLATON.[24]

We then turned our attention to the treatment of **L**-H_4 with Zr^{IV} and Hf^{IV} precursors for the generation of new MOF materials. Growing high quality crystals of Zr-MOFs suitable for single crystal X-ray diffraction (scXRD) studies can be particularly challenging, with Zr-MOFs typically being obtained as polycrystalline solids.[25] It was therefore necessary to employ formic acid as a modulator[26] in order to prepare suitably large single crystals. Thus, treatment of **L**-H_4 with $ZrOCl_2{\cdot}8H_2O$ or $HfCl_4$ in a 2 : 1 mixture of DMF and formic acid at 100 °C for 48 h both afforded colourless needles. These crystals were found by scXRD analysis to comprise isostructural MOFs of the general formula $[M_3O_4(\mathbf{L})(DMF)_4]{\cdot}x$DMF [**IMP-32**-Zr (M = Zr, x = 3) or **IMP-32**-Hf (M = Hf, x = 2)] and phase purity of the bulk samples was verified by powder X-ray diffraction (Fig. S4, ESI†).[27]

In both frameworks, **L**-H_4 has become fully deprotonated under the solvothermal conditions employed with each of its acid groups binding to a separate metal node. The siloxane

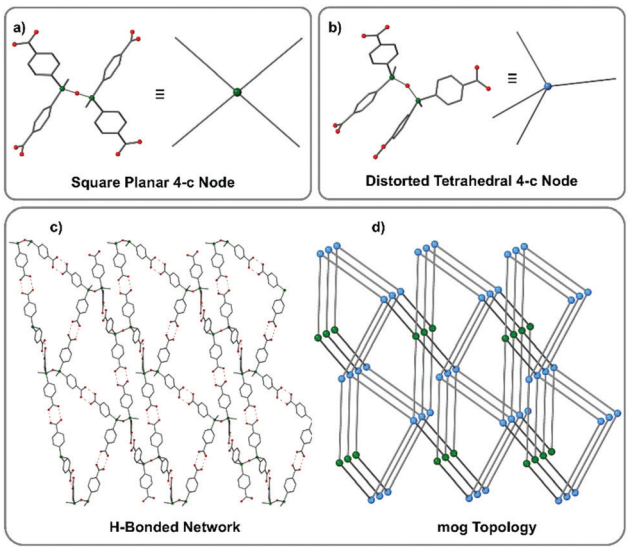

Fig. 1 Linear (a) and bent (b) siloxane molecules in the structure of **L**-H_4 and corresponding geometric simplifications. (c) Portion of the extended structure of a single **mog** net built from **L**-H_4 viewed along the crystallographic *b* axis. H-bonds shown by red dashed lines. Colour scheme: O, red; C, grey; Si, green. (d) Schematic representation of the underlying **mog** network comprised of square planar (green) and distorted tetrahedral (blue) nodes.

linkage is linear with the central siloxane oxygen sitting on a centre of symmetry. The Si–CH_3 groups are in the antiperiplanar conformation and consequently the coordinating branches of **L** are disposed in a manner such that the acid groups are at the corners of a rectangle and thus **L** can be simplified to a square planar 4-c node. The metallic nodes in **IMP-32**-Zr comprise the known 8-connected Zr_6O_8 cluster as seen in a number of reported MOFs.[20] The zirconium atoms sit at the corners of an octahedron where the axial edges are occupied by bridging dimonodentate carboxylate groups from eight different **L** molecules. The coordination sphere of each zirconium atom which sits in the equatorial plane is completed by the additional coordination of two DMF molecules. These 8-connected Zr SBUs are crosslinked by **L** to form a 3D MOF with 4,8-connected **scu** topology, infrequently encountered in Zr-MOFs (see Fig. 2).[28,29] Another topological description of **IMP-32** recognizes the 3-connected branch points centred on the terminal silicon vertices of **L**. This instead gives rise to the extremely rare **scu**-derived 3,8-connected **tty** topology.[30,31]

The **IMP-32**-Zr framework has solvent-filled channels in all directions with the largest window size being approximately 10 × 9 $Å^2$ (centroid to centroid distances) along the crystallographic *a* axis. TGA analysis under N_2 of **IMP-32** MOFs both showed solvent loss occurring between 30–270 °C. The frameworks appear to remain stable until a temperature of approximately 500 °C when the onset of decomposition occurs suggesting high thermal stability (see Fig. S5, ESI†). After theoretical removal of both the coordinated and non-coordinated solvent, the PLATON[24] estimated solvent-accessible void volume for **IMP-32**-Zr was found to be 9074.1 $Å^3$ or 63% of the unit cell volume. The comparable values found for **IMP-32**-Hf are 9023.2 $Å^3$

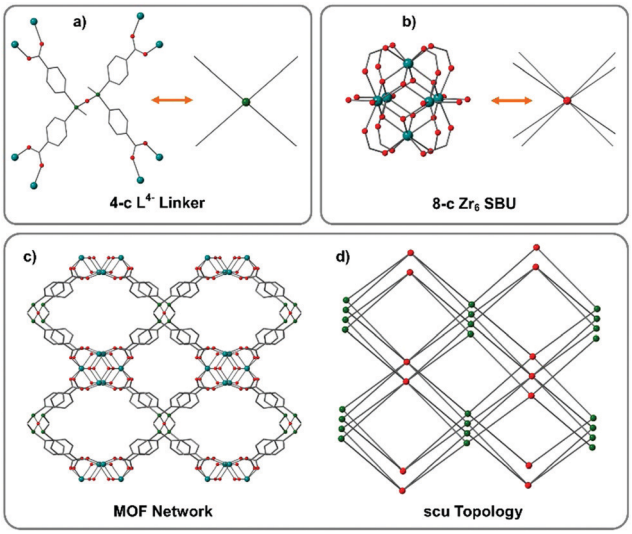

Fig. 2 (a) Ligand environment of **L** in **IMP-32**-Zr. (b) Structure of hexanuclear Zr_6O_8 SBUs in **IMP-32**-Zr. Note only the coordinating O atoms of ligated DMF molecules are shown for clarity. (c) Portion of the extended structure of **IMP-32**-Zr showing pores along the crystallographic *a* axis. Solvent molecules and hydrogen atoms omitted for clarity. Colour scheme: Zr, turquoise; O, red; C, grey; Si, green. (d) Schematic representation of the **scu** network showing the 8-connected Zr_6O_8 SBU nodes (red) and the 4-connected silicon-based nodes (green).

and 63%. The two MOF samples were then subjected to a two-step activation procedure.[32] The as-synthesized material was first soaked in DCM to exchange the DMF molecules included in the pore space. This solvent-exchanged material was subsequently soaked in the lower surface tension solvent *n*-hexane prior to evacuation at room temperature. PXRD measurements on the activated **IMP-32** sample showed retention of crystallinity and N_2 sorption studies on **IMP-32**-Zr show a reversible Type-I adsorption isotherm at 77 K with a calculated BET surface area of 1135 $m^2\ g^{-1}$ while **IMP-32**-Hf was found to possess a BET surface area of 1001 $m^2\ g^{-1}$ (see Fig. S5 and S6, ESI,† respectively).

The robustness of Zr-MOFs is now well established,[20] but there have been comparatively few investigations on water adsorption in these systems with preliminary studies suggesting that many Zr-MOFs take up significant amounts of water and so are prone to becoming saturated.[33] Contrastingly, studies on coordination polymers containing tetramethyldisiloxane groups have revealed hydrophobic behaviour.[34,35] Hence, the incorporation of Si–CH_3 groups in **L**-H_4 was designed to impart an inherent hydrophobicity in **IMP-32** MOFs without the need for hydrophobic coating agents. Dynamic vapour sorption (DVS) studies on **IMP-32** MOFs confirmed their low affinity towards water with both MOFs showing limited (<4 wt%, see Fig. 3) water uptake at relative humidity levels below 20% (relevant for separation of industrial gas streams). Even at 95% relative humidity, the **IMP-32** MOFs show relatively low (≤ 15 wt%) water uptake placing them among the lowest reported H_2O-adsorbing MOFs when compared to materials of similar surface areas.[36,37]

The aqueous stability of MOFs is crucial to their applications in gas separations in humid environments, for example in

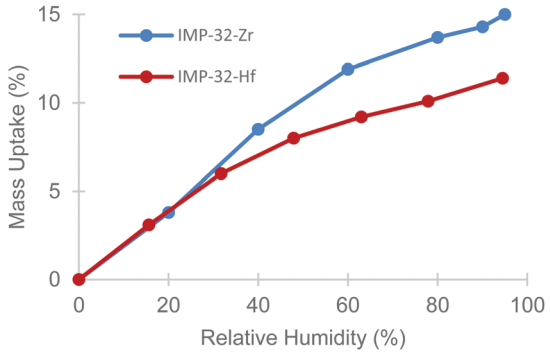

Fig. 3 Water vapour adsorption isotherms for **IMP-32** MOFs at 23 °C.

post-combustion carbon capture and storage systems. The aqueous stability of **IMP-32**-Zr was thus further examined by immersing samples of the MOF in water or 1 M HCl for 24 hours. In both cases no change in crystallinity was observed as evidenced by PXRD (see Fig. S8, ESI†). However, **IMP-32**-Zr was shown to degrade in the presence of 1 M NaOH forming an amorphous solid. This is explained by the fact that the **L**-H_4 building block is readily cleaved by base to afford bis(*p*-carboxyphenyl)methylsilanol (see ESI,† for further details). Efforts to crystallize this silanol led to self-condensation re-forming **L**-H_4. Studies on the coordination behaviour and application of this novel silanol are ongoing.

The CO_2 uptake capacity of the **IMP-32** MOFs at 25 °C between 0–1 bar was next investigated. These studies reveal a reversible Type-I CO_2 adsorption isotherm (see Fig. 4) with an uptake of 5.9 wt% in **IMP-32**-Zr and 5.2 wt% in **IMP-32**-Hf. Thus **IMP-32** MOFs show promising CO_2 capture performance when compared to other known low water affinity frameworks.[38]

In summary, the novel siloxane-based tetracarboxylic acid **L**-H_4 has been prepared and shown to self-assemble into a quadruply interpenetrated 3D supramolecular network. Treatment of **L**-H_4 with Zr^{IV} and Hf^{IV} precursors gave **IMP-32**-Zr/Hf which are the first Zr/Hf-MOFs incorporating siloxane-based linkers. These linkers are demonstrated to impart the resultant MOFs with very low water affinity without compromising their

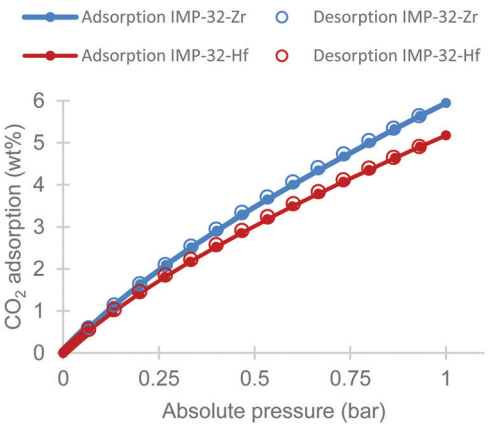

Fig. 4 CO_2 sorption isotherms for **IMP-32** MOFs at 25 °C.

porosity. In addition, the **IMP-32** series represents an important addition to the rare list of MOFs with the **scu**-derived **tty** topology highlighting the versatility of organosilicon compounds in topology-guided synthesis of 3D MOF structures. Encouraged by the low water affinity of **IMP-32** MOFs we are interested in further investigating the effectiveness of siloxane-based MOFs in the capture of a wide range of pollutants from ambient air and aqueous solution.

The Imperial College President's Scholarship Scheme (L. D.) and the EPSRC (EP/M507878/1) are acknowledged for funding this work. We are grateful to Camille Petit (Imperial College London) for assistance with BET measurements. We thank the EPSRC UK National Crystallography Service at the University of Southampton for the collection of the crystallographic data.

Conflicts of interest

There are no conflicts to declare.

Notes and references

1 P. Puthiaraj, Y.-R. Lee, S. Ravi, S. Zhang and W.-S. Ahn, *Post-combustion Carbon Dioxide Capture Materials*, The Royal Society of Chemistry, London, 2019, pp. 153–205.
2 O. M. Yaghi, M. J. Kalmutzki and C. S. Diercks, *Introduction to Reticular Chemistry: Metal-Organic Frameworks and Covalent Organic Frameworks*, Wiley-VCH, Weinheim, 2019.
3 S. Kaskel, *The chemistry of metal-organic frameworks: synthesis, characterization, and applications*, Wiley-VCH, Weinheim, 2016.
4 C. Wang, X. Liu, N. Keser Demir, J. P. Chen and K. Li, *Chem. Soc. Rev.*, 2016, **45**, 5107–5134.
5 K. Jayaramulu, F. Geyer, A. Schneemann, Š. Kment, M. Otyepka, R. Zboril, D. Vollmer and R. A. Fischer, *Adv. Mater.*, 2019, **31**, 1900820.
6 W. Zhang, Y. Hu, J. Ge, H.-L. Jiang and S.-H. Yu, *J. Am. Chem. Soc.*, 2014, **136**, 16978–16981.
7 G. Huang, Q. Yang, Q. Xu, S. H. Yu and H. L. Jiang, *Angew. Chem., Int. Ed.*, 2016, **55**, 7379–7383.
8 X. Qian, F. Sun, J. Sun, H. Wu, F. Xiao, X. Wu and G. Zhu, *Nanoscale*, 2017, **9**, 2003–2008.
9 C. A. Fernandez, S. K. Nune, H. V. Annapureddy, L. X. Dang, B. P. McGrail, F. Zheng, E. Polikarpov, D. L. King, C. Freeman and K. P. Brooks, *Dalton Trans.*, 2015, **44**, 13490–13497.
10 C. Yang, U. Kaipa, Q. Z. Mather, X. Wang, V. Nesterov, A. F. Venero and M. A. Omary, *J. Am. Chem. Soc.*, 2011, **133**, 18094–18097.
11 R. Navarro Amador, L. Cirre, M. Carboni and D. Meyer, *J. Environ. Manage.*, 2018, **214**, 17–22.
12 P. Ji, T. Drake, A. Murakami, P. Oliveres, J. H. Skone and W. Lin, *J. Am. Chem. Soc.*, 2018, **140**, 10553–10561.
13 J. Krautwurst, D. Smets, R. Lamann and U. Ruschewitz, *Inorg. Chem.*, 2019, **58**, 8622–8632.
14 E. M. Sunderland, X. C. Hu, C. Dassuncao, A. K. Tokranov, C. C. Wagner and J. G. Allen, *J. Exposure Sci. Environ. Epidemiol.*, 2019, **29**, 131–147.
15 L. C. Delmas, P. N. Horton, A. J. P. White, S. J. Coles, P. D. Lickiss and R. P. Davies, *Polyhedron*, 2019, **157**, 25–32.
16 L. C. Delmas, A. J. P. White, D. Pugh, P. N. Horton, S. J. Coles, P. D. Lickiss and R. P. Davies, *CrystEngComm*, 2018, **20**, 4541–4545.
17 L. C. Delmas, P. N. Horton, A. J. P. White, S. J. Coles, P. D. Lickiss and R. P. Davies, *Chem. Commun.*, 2017, **53**, 12524–12527.
18 W. Noll, *Chemistry and Technology of Silicones*, Academic Press, London, 2012.
19 D. Sun, P. R. Adiyala, S.-J. Yim and D.-P. Kim, *Angew. Chem., Int. Ed.*, 2019, **58**, 7405–7409.
20 Y. Bai, Y. Dou, L.-H. Xie, W. Rutledge, J.-R. Li and H.-C. Zhou, *Chem. Soc. Rev.*, 2016, **45**, 2327–2367.
21 R.-B. Lin, Y. He, P. Li, H. Wang, W. Zhou and B. Chen, *Chem. Soc. Rev.*, 2019, **48**, 1362–1389.
22 I. Hisaki, C. Xin, K. Takahashi and T. Nakamura, *Angew. Chem.*, 2019, **131**, 1160–11170.
23 I. Hisaki, *J. Inclusion Phenom. Macrocyclic Chem.*, 2020, **96**, 215–231.
24 A. L. Spek, *J. Appl. Crystallogr.*, 2003, **36**, 7–13.
25 R. J. Marshall, C. L. Hobday, C. F. Murphie, S. L. Griffin, C. A. Morrison, S. A. Moggach and R. S. Forgan, *J. Mater. Chem. A*, 2016, **4**, 6955–6963.
26 S. Wang, J. Wang, W. Cheng, X. Yang, Z. Zhang, Y. Xu, H. Liu, Y. Wu and M. Fang, *Dalton Trans.*, 2015, **44**, 8049–8061.
27 S. J. Coles and P. A. Gale, *Chem. Sci.*, 2012, **3**, 683–689.
28 Y. Wang, L. Feng, K. Zhang, K.-Y. Wang, W. Fan, X. Wang, B. Guo, F. Dai, L. Zhang, D. Sun and H.-C. Zhou, *Adv. Sci.*, 2019, **6**, 1901855.
29 H. Wang, X. Dong, J. Lin, S. J. Teat, S. Jensen, J. Cure, E. V. Alexandrov, Q. Xia, K. Tan, Q. Wang, D. H. Olson, D. M. Proserpio, Y. J. Chabal, T. Thonhauser, J. Sun, Y. Han and J. Li, *Nat. Commun.*, 2018, **9**, 1745.
30 T.-P. Hu, Z.-J. Xue, B.-H. Zheng, X.-Q. Wang, X.-N. Hao and Y. Song, *CrystEngComm*, 2016, **18**, 5386–5392.
31 X. Cui, M.-C. Xu, L.-J. Zhang, R.-X. Yao and X.-M. Zhang, *Dalton Trans.*, 2015, **44**, 12711–12716.
32 J. Ma, A. P. Kalenak, A. G. Wong-Foy and A. J. Matzger, *Angew. Chem., Int. Ed.*, 2017, **56**, 14618–14621.
33 H. Furukawa, F. Gándara, Y.-B. Zhang, J. Jiang, W. L. Queen, M. R. Hudson and O. M. Yaghi, *J. Am. Chem. Soc.*, 2014, **136**, 4369–4381.
34 C. Racles, M.-F. Zaltariov, M. Iacob, M. Silion, M. Avadanei and A. Bargan, *Appl. Catal., B*, 2017, **205**, 78–92.
35 A. Vlad, M.-F. Zaltariov, S. Shova, G. Novitchi, C.-D. Varganici, C. Train and M. Cazacu, *CrystEngComm*, 2013, **15**, 5368–5375.
36 H. Jasuja, J. Zang, D. S. Sholl and K. S. Walton, *J. Phys. Chem. C*, 2012, **116**, 23526–23532.
37 Y. Huang, W. Qin, Z. Li and Y. Li, *Dalton Trans.*, 2012, **41**, 9283–9285.
38 C. A. Trickett, A. Helal, B. A. Al-Maythalony, Z. H. Yamani, K. E. Cordova and O. M. Yaghi, *Nat. Rev. Mater.*, 2017, **2**, 17045.

